

Comparison of Radar Data from the TRMM Satellite and Kwajalein Oceanic Validation Site

COURTNEY SCHUMACHER AND ROBERT A. HOUZE JR.

Department of Atmospheric Sciences, University of Washington, Seattle, Washington

(Manuscript received 4 October 1999, in final form 13 April 2000)

ABSTRACT

Data from the Tropical Rainfall Measuring Mission (TRMM) precipitation radar (PR) and Kwajalein S-band validation radar (KR) agree well for reflectivity exceeding the sensitivity of the PR threshold (~ 17 dBZ). For echoes above this intensity threshold, the products derived from reflectivity, particularly maps of rainfall rate and convective/stratiform classification, compare well, even though slightly different convective–stratiform separation techniques and different reflectivity–rainfall rate (Z – R) relations are used for the PR and KR. The KR observations indicate the PR misses only 2.3% of near-surface rainfall but 46% of near-surface rain area (≥ 0 dBZ) because of its 17-dBZ threshold. The PR senses less than 15% of the echo area observed by the KR above 5-km altitude (i.e., above the 0°C level). Thus, the PR highly undersamples weaker echoes associated with stratiform rain near the surface and ice particles aloft but still manages to capture most of the near-surface precipitation accumulation. The temporal sampling of the TRMM PR accurately captures the KR's overall frequency distribution of reflectivity and its subdivision into convective and stratiform components. However, diurnal and latitudinal variations of precipitation in the vicinity of Kwajalein are not well sampled.

1. Introduction

The primary goal of the Tropical Rainfall Measuring Mission (TRMM) is to determine the four-dimensional distribution of latent heating in the Tropics (Simpson et al. 1988). To achieve this goal, the low-altitude, low-inclination TRMM spacecraft launched in November 1997 had an active precipitation radar (PR) on board, along with a multichannel passive TRMM Microwave Imager (TMI), visible and infrared scanner, Clouds and Earth's Radiant Energy System, and Lightning Imaging Sensor. The PR is crucial to the mission because of its ability to detect the precipitation field with high resolution in both the horizontal and vertical. The TRMM satellite is ~ 350 km above the earth's surface, and the PR scans 17° to either side of nadir at intervals of 0.35° (Table 1). This geometry provides data over a swath 215 km wide at the earth's surface, with a horizontal footprint of ~ 4 km and a vertical resolution of 250 m at nadir.

Operating at a frequency of 13.8 GHz (2.17-cm wavelength), the PR is subject to strong attenuation. In addition, the radar has a relatively low sensitivity, detecting echoes of only 17 dBZ and higher. Occasionally,

the PR captures meteorological phenomena at reflectivities less than 17 dBZ, but the signal-to-noise ratio at those lower reflectivities is weak. The beam of the PR is always within 17° of vertical and is reflected by the earth's surface. The reflectivity profile in each beam is corrected for attenuation by a hybrid method based on the method of Hitschfeld and Bordan (1954), which uses a calibrated constant to account for attenuation in estimating rain rate from returned power at a given range, and the technique of Iguchi and Meneghini (1994), which uses the reflectivity of the earth's surface as a reference value. An assumption regarding the drop size distribution of the rain detected by the radar together with a clear-air observation of the surface reflectivity leads to an estimate of the attenuation of the surface echo seen through rain. This estimate is the basis for correcting the observed reflectivity for attenuation as a function of range. Steiner and Houze (1998) showed that, without a correction for attenuation, the PR data are probably only reliable at heights of ~ 5 – 7 km above mean sea level (i.e., at and just above the melting level).

Because of the limitations imposed by sensitivity and attenuation, it is important to compare the PR data with the data of a highly sensitive three-dimensionally scanning S-band (i.e., nonattenuated) radar. The radar at the Kwajalein TRMM validation site provides a useful oceanic dataset for comparison. Kwajalein is the only permanent validation site where ground-based coverage is almost entirely over water. Because passive microwave

Corresponding author address: Courtney Schumacher, Dept. of Atmospheric Sciences, University of Washington, Box 351640, Seattle, WA 98195-1640.
E-mail: courtney@atmos.washington.edu

TABLE 1. Characteristics of the TRMM PR and Kwajalein radar.

	PR	KR
Frequency/wavelength	13.8 GHz/2.17 cm (K_u band)	2.8 GHz/10.71 cm (S band)
Beamwidth	0.71°	1.12°
Peak transmit power	500 W	500 kW (250 kW horizontal, 250 kW vertical)
Horizontal (h) and vertical (v) resolution	h = 4.3 km (nadir) v = 0.25 km (nadir)	h = 0.25 km (gate spacing) v = varies (interpolated to 1 km)
Horizontal range	215 km (swath width)	150 km (radius from radar)
Pulse duration	1.6 μ s	0.72 μ s
Minimum detectable signal	~17 dBZ	-108 dBm
Doppler	no	yes
Pulse repetition frequency	2776 Hz	960 Hz interspersed with 396 Hz
Antenna height above mean sea level	350 km	24.8 m
Speed of one scan	34° in 0.6 s	360° in 18 s (max)
Scan range	$\pm 17^\circ$ (cross track)	-0.4° to 90.5° (elevation)

rain algorithms operate much differently over ocean than over land, Kwajalein stands as a unique validation site for TRMM. The characteristics of the Kwajalein radar (KR, Table 1) are similar to the well-known Weather Surveillance Radar-1988 Doppler (WSR-88D) Next-Generation Weather Radar (NEXRAD) radars used by the U.S. National Weather Service. However, because the KR is a TRMM facility, it was not constrained to the scan strategy of the NEXRAD radars. It therefore was possible to design scan strategies that produce higher vertical resolution data, comparable to the high vertical resolution of the TRMM PR reflectivity fields.

The purpose of this paper is to report on comparisons

of the PR and KR data that have been collected since the launch of the TRMM satellite. These comparisons indicate that the attenuation correction generally works well but the limited sensitivity of the PR biases the satellite's measurements toward convective precipitation. A small percentage of precipitation but a much larger percentage of precipitation area cannot be seen by the TRMM PR. The large areas of low-reflectivity precipitation are weak stratiform areas that, even with their very low rain rates, can cover large areas and significantly affect latent heating and radiative heating profiles in the atmosphere (Houze 1982, 1989). In addition, climatological observations are severely limited by the temporal sampling of the TRMM satellite.

2. The Kwajalein oceanic validation site

Kwajalein Atoll is part of the Marshall Islands, which are on the eastern edge of the western Pacific warm pool. The KR is located at the southern tip of the Kwajalein Atoll on Kwajalein Island (8.7°N, 167.7°E), and the validation area is defined as the 150-km radius around the radar (Fig. 1). Because Kwajalein Atoll and neighboring atolls are thin strips of land surrounding large lagoons, the area covered by the KR is nearly 100% oceanic. The KR is an S-band, dual-polarization, Doppler weather radar with a beamwidth of 1.12° (Table 1). The scan strategy has 17–22 elevation angles. This strategy maximizes vertical resolution within the Kwajalein validation area. Radar data are quality controlled using an algorithm developed by the Mesoscale Group at the University of Washington. This algorithm looks at textures of the base reflectivity field and continuity between lower-level tilts to detect and to remove clutter and other nonmeteorological echoes. Strong ground clutter, anomalous propagation, and second-trip echoes¹

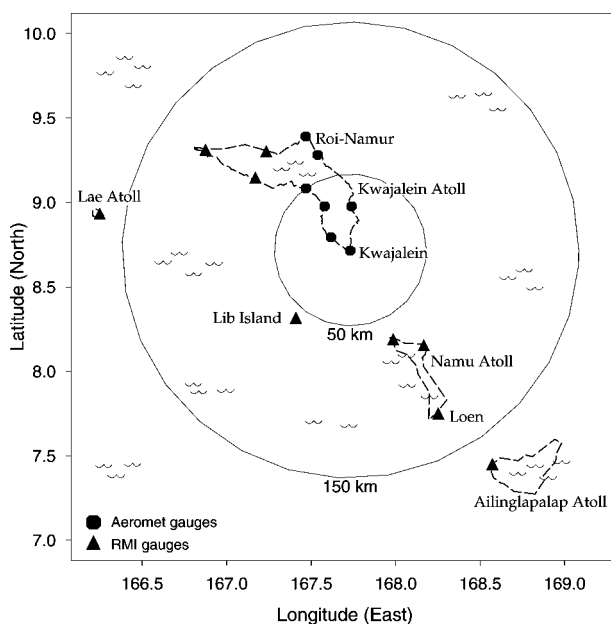


FIG. 1. Map of the Kwajalein area centered on the KR. The geography of the Kwajalein Atoll and neighboring atolls are indicated by dashed lines. The interior of each atoll is a giant lagoon; thus the area covered by the radar is almost all open ocean. Rain gauge locations are indicated by the key for each network.

¹ Because of the low pulse-repetition frequency required for Doppler velocity measurements, long-range echoes from a previous pulse may be received along with the return of the subsequent pulse. Distant echoes can thus be plotted incorrectly close to the radar. These falsely plotted echoes are called second-trip echoes.

TABLE 2. PR and Kwajalein gauges in comparison with the KR.

Aug 1998–May 1999				Jun–Aug 1999			
dB offset	Σ PR/ Σ KR	Median PR/KR	Median gauge/KR	dB offset	Σ PR/ Σ KR	Median PR/KR	Median gauge/KR
0	1.33	1.37	2.2	0	1.75	2.05	5.2
+1	1.18	1.24	1.8	+4	1.09	1.26	2.3
+2	1.05	1.12	1.5	+5	0.98	1.11	1.9
+3	0.94	0.99	1.2	+6	0.87	0.99	1.5
+4	0.84	0.89	1.0	+7	0.77	0.89	1.3
				+8	0.70	0.79	1.0

that extend into the second and third tilts are only partially removed. Sea clutter and second-trip echoes are the prevalent nonmeteorological returns at Kwajalein. The quality control generally removes the sea clutter but does not always eradicate second-trip echoes.

The Kwajalein validation site has small networks of Qualimetrics, Inc., tipping-bucket rain gauges operated by Aeromet, Inc., and the Republic of the Marshall Islands (RMI). Seven Aeromet and 10 RMI gauges are located within a 200-km radius of the radar (Fig. 1). The gauges measure 0.25 millimeters per tip and record tips every 15 s in the Aeromet network and 10 s in the RMI network. Ten of the 17 tipping-bucket rain gauges regularly report data. Typically only five to six of these 10 gauges provide a complete record for a month. We flagged as incomplete any months that were obviously missing data or seem to have had large gaps when compared with surrounding gauges. If there were more than four tips in a 10-s period or five tips in a 15-s period (equal to rain rates greater than 300 mm h^{-1}), the data were usually removed.

3. Calibration of the KR

The calibration of the KR, although generally stable, can shift as a result of repairs, upgrades, and other factors. Both the Kwajalein gauges and the PR provide independent, stable time series by which to track the calibration of the KR. There were two distinct calibration periods between August 1998 and August 1999 separated by major upgrades and repairs made to the KR during late May to late June 1999. The KR calibration was low in comparison with the PR and Kwajalein gauges for both periods but was significantly lower during the second period. An official calibration offset for the second period, which includes the Kwajalein Experiment, is in the process of being defined. However, a preliminary calibration estimate brings the KR within 1–2 dB of its appropriate measurements for both periods, which is sufficient for the analyses of this paper.

Two steps were involved in the preliminary KR calibration estimates. The first step compared areal coverage by PR and KR echo ≥ 17 dBZ for the 50 overpasses. The second step compared rain gauge and KR monthly rain accumulations. A total of 34 overpasses occurred during the first period (August 1998–May

1999); 16 overpasses occurred during the second period (June–August 1999).

PR and KR echo areas ≥ 17 dBZ at 1-km height intervals from 3 to 15 km were accumulated for the 50 overpass cases. Table 2 shows ratios of PR to KR total areas for each period at varying calibration offsets. Σ PR/ Σ KR represents the ratio of total echo area ≥ 17 dBZ seen by the PR to that seen by the KR for the entire period. Median PR/KR represents the median of individual overpass PR/KR echo areas. Σ PR/ Σ KR weights the larger overpasses more heavily; the median PR/KR weights each overpass equally. There tends to be a greater percent difference between the PR and KR for overpasses with less rain so the median PR/KR requires higher offsets to approach 1. The ratios indicate a KR offset between +2 and +3 dB for the first period and between +5 and +6 dB for the second period.

Kwajalein gauge accumulations were compared with the reflectivity values of the $2 \text{ km} \times 2 \text{ km}$ pixel above the gauge in the lowest tilt (usually 0.4°) of the KR. The complete KR dataset was used instead of just the overpass subset. When there was rain at both the gauge and the radar pixel above the gauge, 10 min of gauge data centered on the radar observation time were summed, and the radar rain rate was assumed to exist for 10 min. The 10-min gauge and radar amounts were then accumulated for monthly amounts of radar-estimated rainfall and gauge-estimated rainfall. The median ratio of gauge to KR monthly rain accumulations for both periods at varying calibration offsets is shown in Table 2. Various factors influence the derivation of surface rain from radar reflectivity; the most important is the height of the radar beam above the surface (Joss and Waldvogel 1990). This factor typically leads to underestimation of surface rainfall by the radar and is not taken into account in the KR values. Therefore, gauge/KR should be greater than 1. Monthly gauge/KR values for well-calibrated months tend to be between 1.5 and 2. The Kwajalein gauge data can be erratic and sparse, so care should be taken when using the gauge/KR values quantitatively. The gauge/KR values suggest a KR offset of +1–2 dB for the first period and +5–6 dB for the second period.

Based on this analysis of both PR and Kwajalein gauge data, our preliminary KR calibration estimate is +2 dB before June 1999 and +6 dB after June 1999.

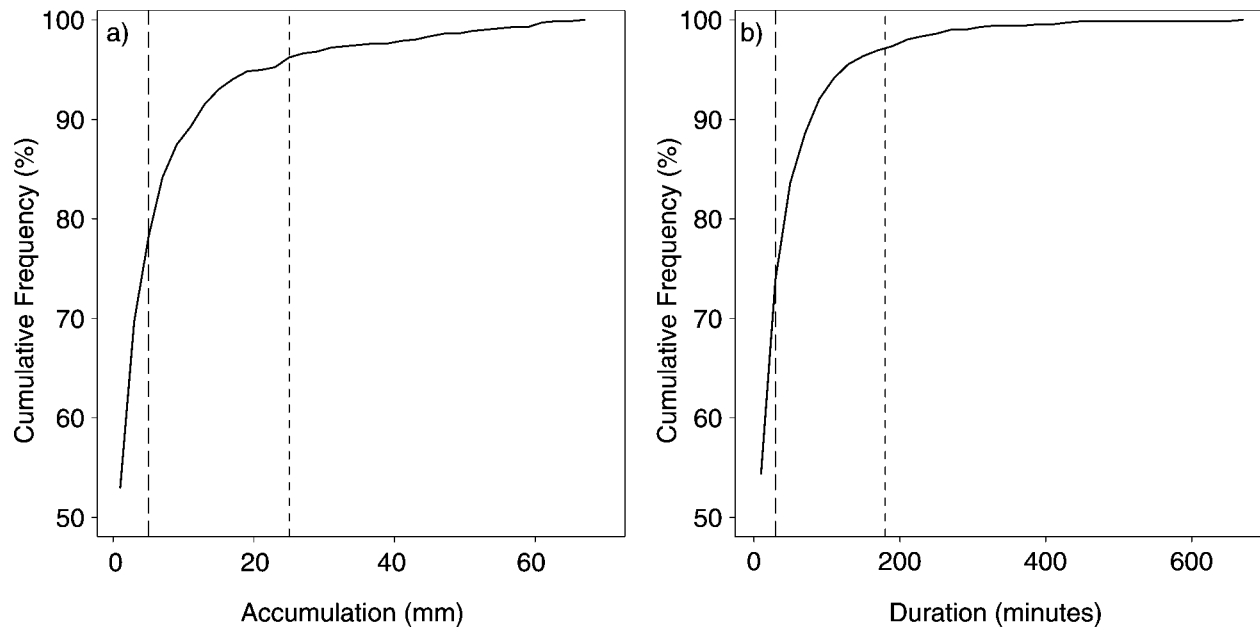


FIG. 2. (a) Cumulative frequency plot for rain-event accumulations at Kwajalein, using Kwajalein Island rain gauge from Mar 1997 to Mar 1999. Vertical lines mark 5 and 25 mm. (b) Cumulative frequency plot for rain-event durations. Vertical lines mark 30 and 180 min.

To indicate the range of uncertainty in these adjustments, in the following sections of this paper we present results for the corrections of +2 and +6 dB and state how much the results would be affected if an additional ± 2 -dB adjustment was made for each time period. The -2 -dB reduction makes the offset 0 before and 4 after June 1999, which leads to median PR/KR ratios of 1.37 and 1.26, respectively (Table 2). We suggest that this 30% difference is unacceptable. The +2-dB increase makes the offset 4 before and 8 after June 1999, leading to median gauge/KR ratios of ~ 1 , which we suggest is too small, for reasons discussed above. Thus the calibration adjustments of 2 ± 2 dB and 6 ± 2 dB before and after June 1999 represent the range of optimal comparisons of the KR with both the PR and the rain gauge networks.

It may seem odd to adjust the KR to agree with the PR, given that the former is a ground-validation radar. However, this adjustment does not diminish the role of the KR. No ground radar in existence has absolute calibration of rain estimates. The usefulness to TRMM of ground-based radars such as the KR is in 1) their high sensitivity and absence of attenuation, which allow accurate characterization of the frequency distribution of reflectivity as a function of altitude and 2) their continuous sampling at a fixed location. These characteristics allow the KR to assess the echo missed by the PR because of sensitivity, attenuation, or sampling.

4. Kwajalein rain events

For 8 months of the year (May–December), Kwajalein receives over 200 mm of rain per month. Tipping-

bucket rain gauge data at Kwajalein Island for March 1997–March 1999 were separated into individual events, defined as having a minimum of two tips and no more than 30 min between tips. There were 719 events over two years. Cumulative frequency plots of rain-event accumulations and rain-event durations for this period indicate that rain events at Kwajalein are generally short lived and intense, with only a small percentage lasting for longer periods and accumulating large amounts of rain. The cumulative frequency plot of rain-event accumulations shows 75% of the events accumulate less than 5 mm (Fig. 2a). For the most significant 25% of events, the curve shifts and approaches an asymptote—only 4% of events achieve accumulations greater than 25 mm (1 in.). The maximum event accumulation was 68 mm. In the cumulative frequency plot of rain-event durations, 75% of events last less than 30 min. Only 3% of events are longer than 3 h (Fig. 2b). The maximum event duration was 11 h. These calculations are consistent with radar data for the same 2-yr period in which echoes were generally isolated, convective, and short lived. Long-lasting systems that create large stratiform areas occur infrequently.

A dearth of events limited validation of the TRMM PR at Kwajalein during the first months of the mission. The 215-km swath of the PR overlaps the 150-km radius around the ground radar 15–20 times each month. Only half of these swaths cover more than 50% of the validation area, and, of these, only a few actually occur when significant rain is present. For example, Fig. 3 shows overpasses in September 1998, climatologically a rainy month. The KR echo is overlaid in black. In addition, a drought during January–June 1998 exacer-

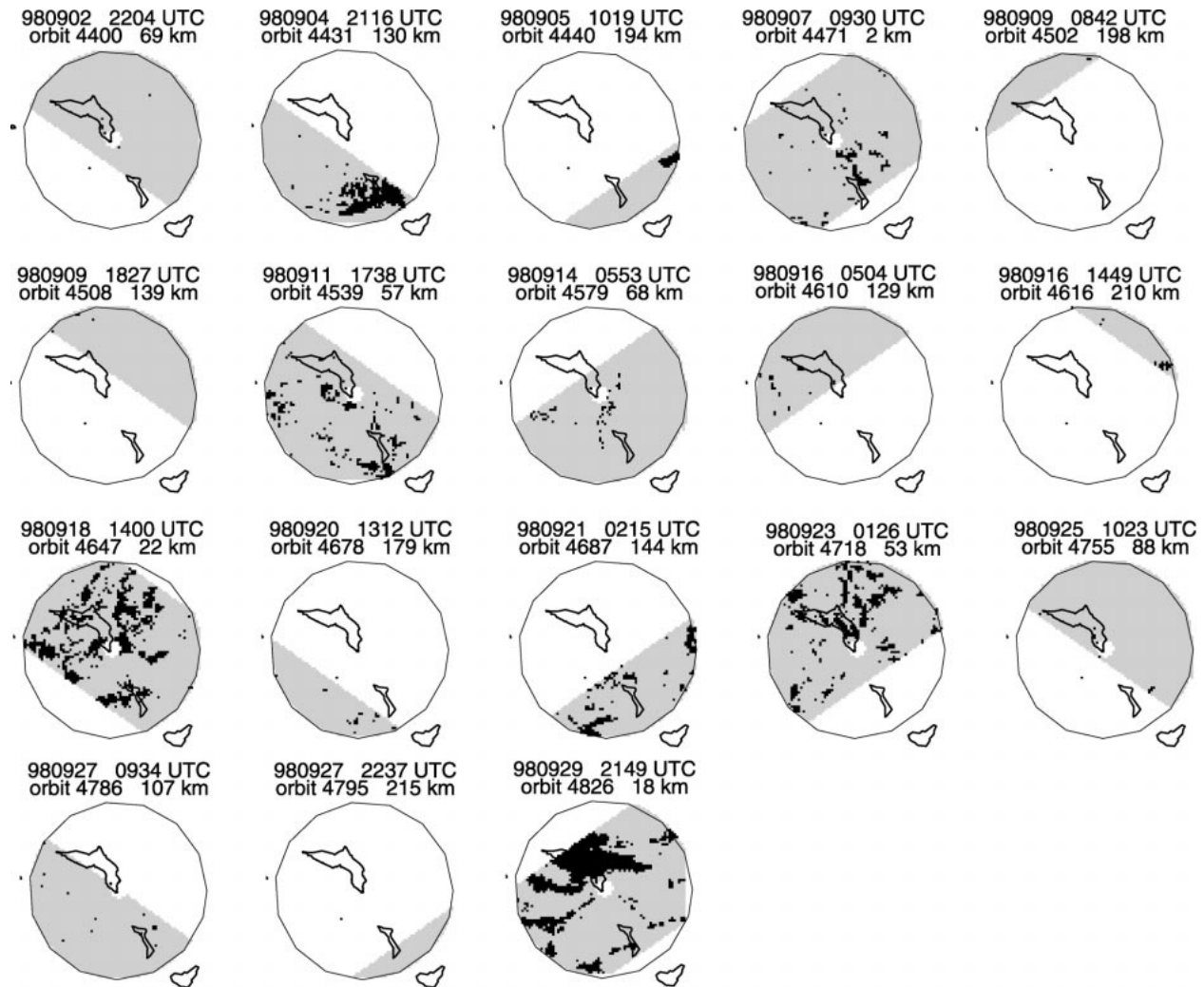


FIG. 3. PR swaths over Kwajalein for Sep 1998. Circle radius is 150 km, centered on the KR. KR echo is outlined in black. Date, time, orbit number, and distance of subsatellite point from the validation radar are indicated for each overpass.

bated the limited opportunity for PR/KR comparisons. Average rain-gauge monthly accumulations were less than 40 mm for that period with only one exception. June averaged 100 mm, which was still well below climatological values of 245 mm. As a result, events for comparison effectively began in the second half of 1998. Fifty events between August 1998 and August 1999 had significant PR/KR overlap and precipitation (at the time of writing, www.atmos.washington.edu/gcg/MG/KWAJ/ had detailed information on each overpass). The following sections present statistical analyses of all 50 cases along with a brief case study of orbit 5712.

5. Reflectivity comparisons

At 0251 UTC 25 November 1998, the TRMM satellite passed within 97 km of the Kwajalein radar (orbit 5712). The 3-km pattern of reflectivity interpolated onto the KR data onto a 4 km \times 4 km Cartesian grid (Fig. 4a)

shows a pattern of relatively small convective cells, some with reflectivity greater than 40 dBZ, interconnected in places by lighter precipitation. The PR 3-km horizontal cross section interpolated onto a 4 km \times 4 km Cartesian grid [TRMM Product Standard Number (TPSN) 2A25, Fig. 4b] is generally consistent with the KR cross section in location and intensity of echo. The PR echo less than 17 dBZ (represented by darker blue and purple) is unconnected and random, indicating noise. The KR has a realistic contiguous low-reflectivity structure. Vertical cross sections constructed at PR ray 28 (Fig. 5) show the convective cells had similar structure and heights; for example the 25-dBZ contour is consistently \sim 5 km for both radars. The PR had a more well-defined bright band in the middle cell (Fig. 5b) because of its greater vertical resolution. In each cross section, the anvil of the cell farthest east is very similar in structure and intensity. Figure 5c is the difference between the attenuation-corrected (TPSN 2A25) and un-

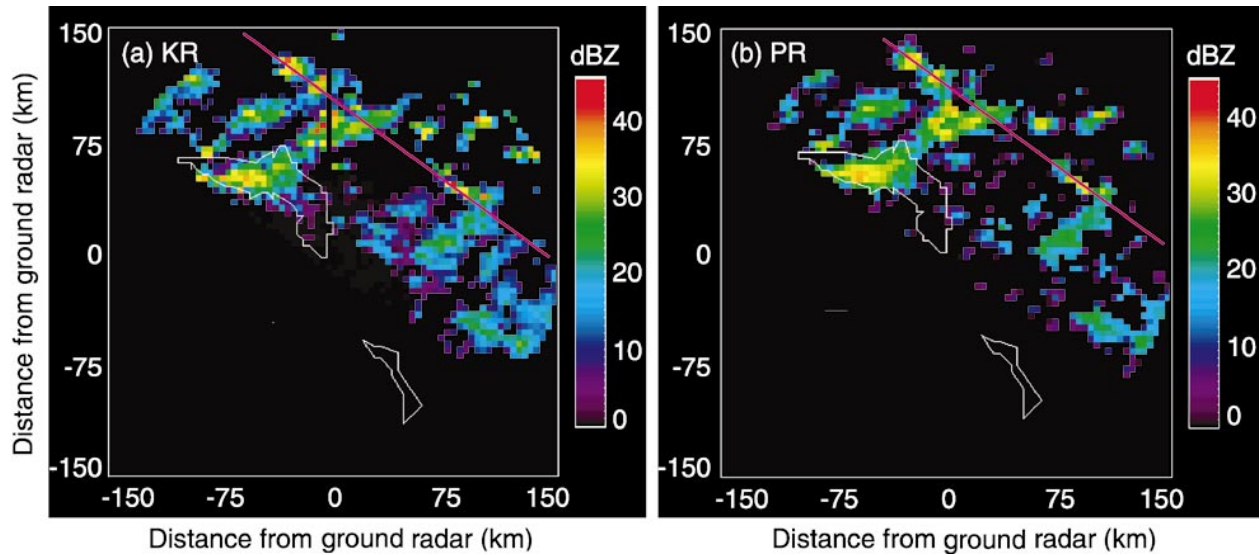


FIG. 4. Convective precipitation case observed at 0251 UTC 25 Nov 1998. The 3-km horizontal cross sections of the (a) KR reflectivity data and (b) PR reflectivity data. The line indicates PR ray 28. The missing beam directly north of the KR occurs in the raw data.

corrected (TPSN 1C21) PR cross sections. The magnitude of the difference at each level is between 0 and 4 dB. Strong convective cells demand the most correction; weaker stratiform areas have need of only small corrections. In addition, the bright band requires some correction.

Histograms of the accumulated echo area versus reflectivity at six different heights for all 50 overpass cases indicate the vertical variation of the PR and KR data at heights up to 8 km (Fig. 6). Weak reflectivities not considered “rain certain” by TPSN 2A25 were removed from the PR histogram counts. The PR does not sense the peaks of the true distributions, which are seen by the KR to be centered at 15–20 dBZ below the 0°C level (Figs. 6a–c), decreasing to 8 dBZ by 8 km (Figs. 6d–f). The KR detects less echo above the 17-dBZ threshold than does the PR at 3, 4, 7, and 8 km. Different wavelengths, sensitivities, scan strategies, and scattering volumes all potentially play a role in offsetting the amount of echo observed by each radar. The distributions agree best at 5 and 6 km, which is consistent with Steiner and Houze’s (1998) conclusion that PR data will be most reliable from 5 to 7 km because the PR highly attenuates below the 0°C level (~5 km), and there are little to no reflectivity data greater than or equal to 17 dBZ observed at heights above 7 km. The amount of echo area

0–16 dBZ in comparison with the total echo area greater than or equal to 0 dBZ (indicating the percent of echo area missed by the PR) is listed in Table 3 for each height in Fig. 6. To explore the sensitivity of the analysis to the KR calibration, Table 3 also includes the percentages assuming an additional ± 2 -dB calibration offset to the KR. A ± 2 -dB offset only marginally affects the results. Below 5 km, the PR detects about half of the echo area. Once above 5 km, the PR misses the majority of the reflectivity field. Table 3 highlights that the low sensitivity of the PR prevents it from detecting widespread, lower-reflectivity precipitation at lower levels and most of the ice region aloft.

6. Classification of rainfall into convective and stratiform categories

The TRMM algorithms used to divide PR and KR echo patterns into convective and stratiform components (TPSNs 2A23 and 2A54, respectively) are based on the horizontal variability of reflectivity (Steiner et al. 1995; Awaka et al. 1997). The PR algorithm contains an additional condition based on the vertical structure of the radar echo. The high vertical resolution (250 m at nadir) and quasi-vertical beam of the PR allow it to identify a bright band for a higher percentage of all echoes than can a quasi-horizontally scanning ground radar; therefore, the PR algorithm uses the presence of the bright band as a primary indicator of stratiform precipitation. The bright band enters the KR convective–stratiform separation only indirectly. The KR algorithm is tuned specifically for Kwajalein, and the presence of the bright band helps to calibrate the horizontal structure analysis.

The KR and PR convective/stratiform maps for orbit 5712 are shown in Fig. 7. The larger convective areas

TABLE 3. KR echo area distribution.

Height (km)	% area 0–16 dBZ	% area		Height (km)	% area 0–16 dBZ	% area	
		+2 dB/–2 dB				+2 dB/–2 dB	
3	51	47/57		6	72	64/79	
4	51	47/57		7	87	80/92	
5	57	52/64		8	94	89/97	

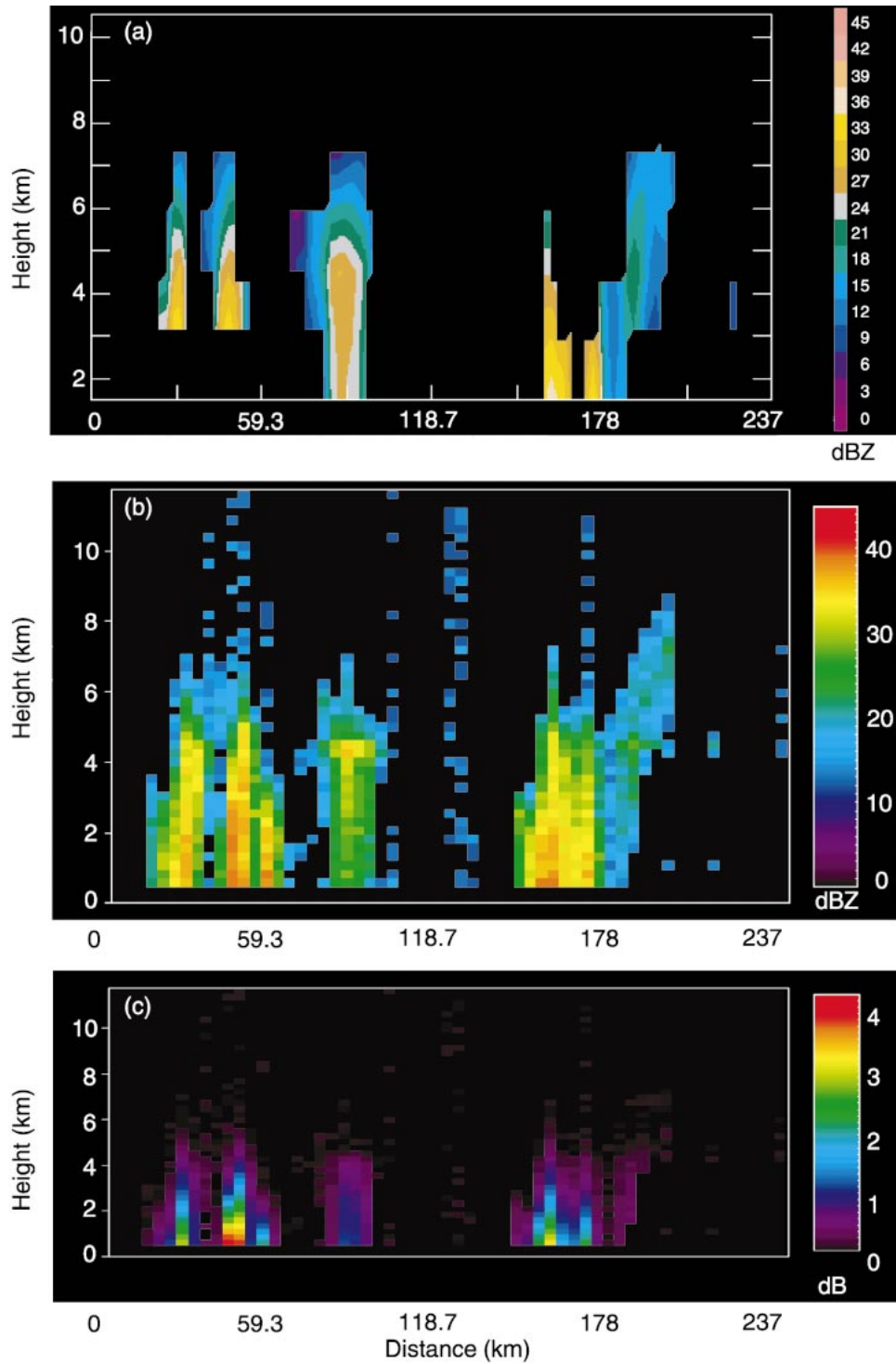


FIG. 5. Vertical cross sections of the case in Fig. 4 at PR ray 28 using (a) interpolated KR reflectivity data, (b) attenuation-corrected PR reflectivity data, and (c) the difference between attenuation-corrected and uncorrected PR reflectivity fields.

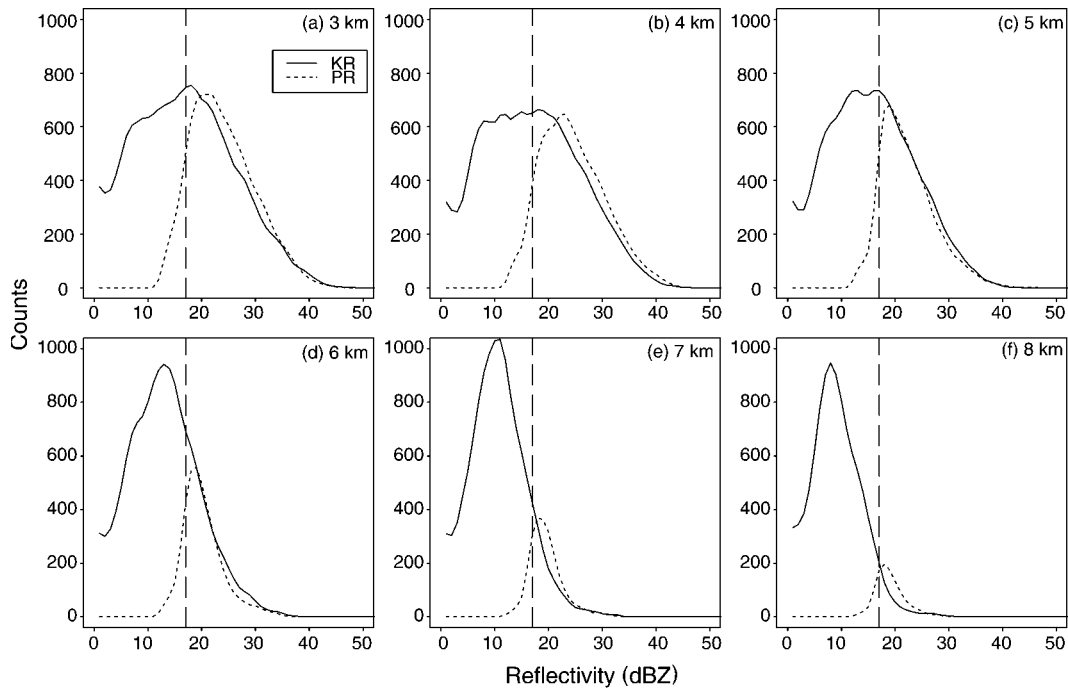


FIG. 6. Histograms of KR and PR reflectivity distributions accumulated at six different heights for the 50 overpass cases. Vertical line marks 17 dBZ to indicate the limit of the PR sensitivity. Counts are total number of $4 \text{ km} \times 4 \text{ km}$ pixels.

match well for the KR and PR maps. However, the KR map identifies more isolated convective elements than does the PR map. This incongruity is either because of the different algorithms or because the KR has higher horizontal resolution than the PR with which to create more accurate $4 \text{ km} \times 4 \text{ km}$ grid values, thus bypassing some of the effects of nonuniform beam-filling. An ad-

ditional difference between the maps is that the PR algorithm has an undecided category, which upon inspection appears to be either stratiform echo or noise. The convective and stratiform rain areas greater than or equal to 17 dBZ for the 50 overpasses (Fig. 8) show that the KR and PR convective/stratiform classifications match well. The ratio of the sum of the individual over-

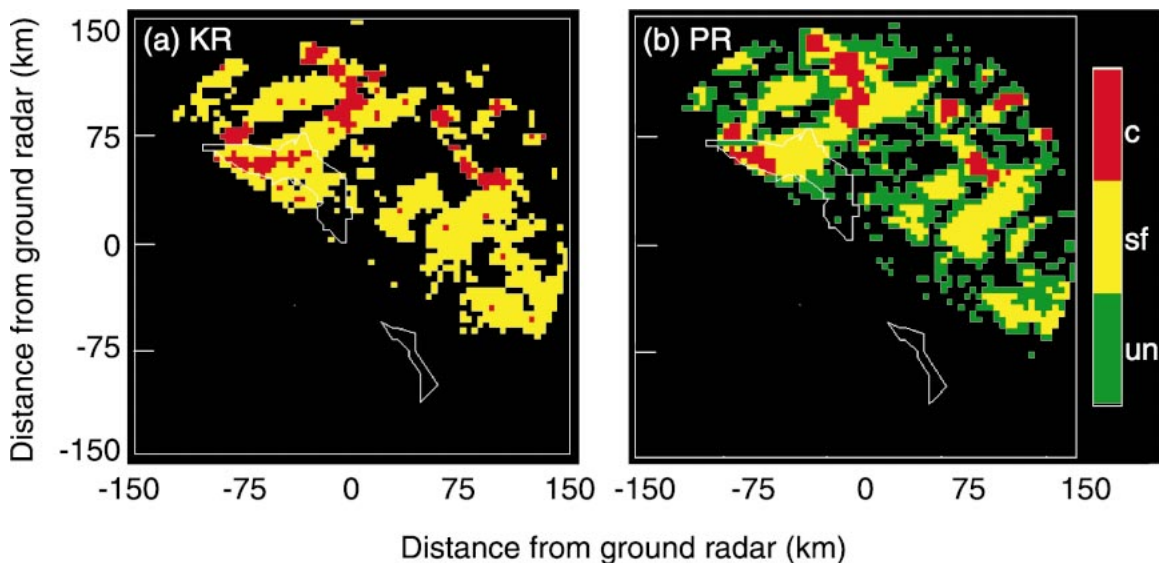


FIG. 7. Convective/stratiform maps for the case in Fig. 4 for (a) KR and (b) PR. The KR convective–stratiform separation utilizes only two categorizations: one for convective, one for stratiform, whereas the PR algorithm has a third, undecided category.

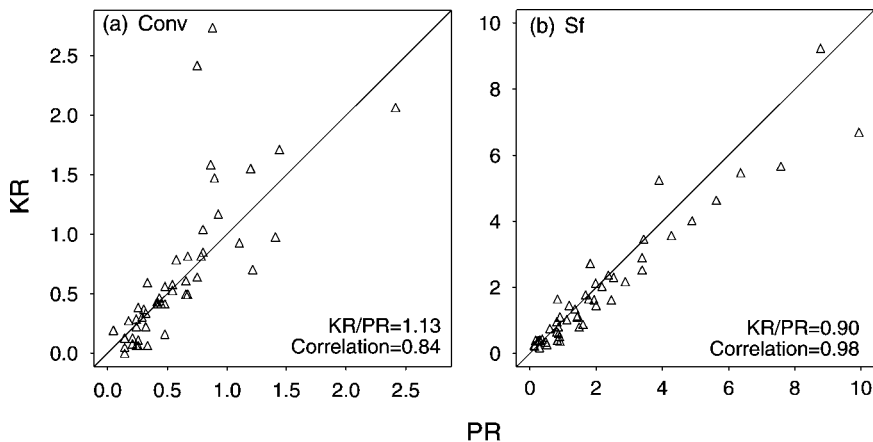


FIG. 8. KR vs PR. (a) Convective and (b) stratiform areas >17 dBZ for all 50 overpasses. KR/PR is the average ratio between individual overpass KR and PR areas. Areas are 10³ km².

pass values (KR/PR) for convective rain area is 1.13 and for stratiform rain area is 0.90; correlations are 0.84 and 0.98, respectively. The KR/PR values and correlations near 1 indicate fairly consistent areal convective/stratiform classification between the two radars. An additional KR calibration offset of +2 dB (-2 dB) increases (decreases) the KR convective rain area by 25% and the KR stratiform rain area by 10%. Therefore, convective rather than stratiform rain areas greater than or equal to 17 dBZ are more sensitive to calibration offsets.

7. Maps of rainfall rate

Near-surface reflectivity *Z* from the KR is converted to rain rate *R* using a single climatological *Z-R* table derived from one year of drop size distribution measurements made on Majuro Atoll from March 1959 to

April 1960 (Mueller and Sims 1967; Fig. 9). Majuro is 427 km southeast of and is similar in climatic regime to Kwajalein Island. The exponential fit to the Mueller and Sims (1967) data is $Z = 293R^{1.26}$ (S. Yuter and W. Parker 2000, personal communication). No coincident radar information was available to classify the drop size distributions as convective or stratiform. The near-surface rain-rate estimates from the TRMM satellite (TPSN 2A25) are calculated using separate convective and stratiform *Z-R* relationships derived from drop size distributions observed near Darwin, Australia. The convective and stratiform *Z-R* relations are $Z = 146R^{1.54}$ and $292R^{1.53}$, respectively (Fig. 9; T. Iguchi 1998, personal communication). The KR and PR *Z-R* relations are generally similar, but the Kwajalein *Z-R* ascribes lower rain rates when *Z* is less than 25 dBZ and higher rain rates when *Z* is greater than 35 dBZ in comparison with the PR *Z-R* relations.

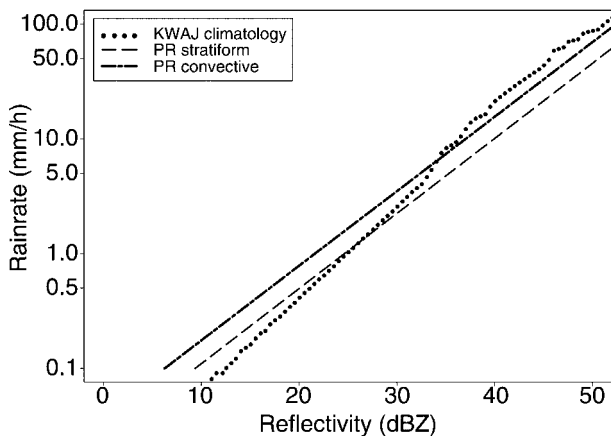


FIG. 9. The *Z-R* relations used for the KR and PR. The single relation of the Kwajalein validation site is based on the climatological drop size distribution from the Marshall Islands, whereas the two relations for the PR are based on disdrometer measurements from Darwin, Australia.

Area-integrated precipitation rates (kg h⁻¹) at 3 km for the PR and KR were calculated for the 50 overpasses using, first, the Kwajalein climatological *Z-R* relation and, then, the respective *Z-R* relations of each instrument (Fig. 10). The KR/PR value for the total precipitation field greater than or equal to 17 dBZ using the Kwajalein *Z-R* relation was 0.99 with a correlation of 0.96, indicating that the KR and PR rain amounts match almost exactly, with little variation (Fig. 10a). The convective component of the KR/PR value was 1.05 (Fig. 10b), whereas the stratiform component was 0.92 (Fig. 10c). Thus the KR and PR convective and stratiform rain amounts both agree within 10%. An additional KR calibration offset of +2 dB (-2 dB) leads to an increase (decrease) of ~60% in KR convective rain amount and ~35% in KR stratiform rain amount. Rain amount is more sensitive to calibration offsets than is rain area.

Calculations applying the PR *Z-R* relation to the PR data gave similar results to using only the Kwajalein *Z-R* relation (Fig. 10). The two PR *Z-R* relations ascribe 7% less rain to PR total rain amounts (2% less to con-

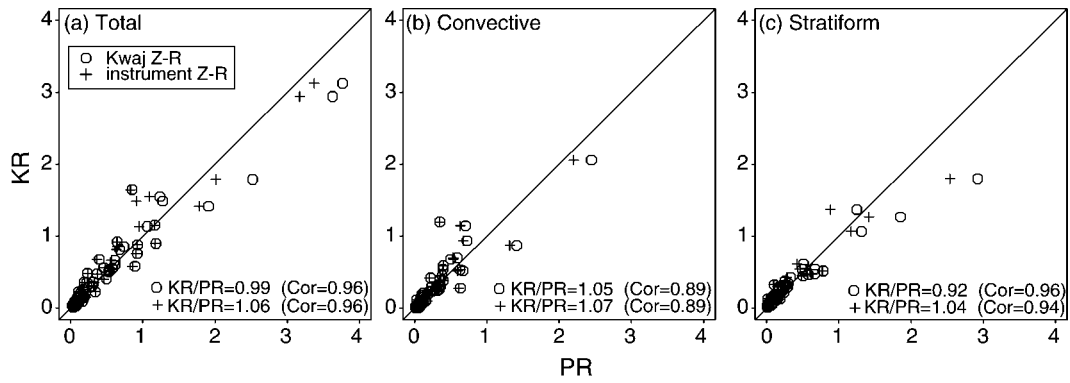


FIG. 10. Area-integrated precipitation rate ($10^{10} \text{ kg h}^{-1}$) for the KR and PR. The KR/PR values represent the average ratio between individual overpass KR and PR area-integrated precipitation rates.

vective events and 13% less to stratiform events) than does the single Kwajalein $Z-R$ relation.

8. Overpass sampling of long-term reflectivity distributions

Previous sections focused on instantaneous comparisons between the KR and PR. Now we address temporal sampling by the TRMM satellite. To simplify processing, the lowest tilt in the KR scan strategy (usually 0.4°) was used in the following analyses as opposed to a

constant height cross section (thus we avoid interpolating the full set of 17–22 elevation angles obtained at each observation time). We extracted the KR data delineated by the 50 overpass swaths of the PR and compared them with the complete KR distribution from August 1998 to August 1999 (Fig. 11).

The frequency distributions of KR echo area versus near-surface reflectivity show a distribution with a peak of reflectivity between 10 and 15 dBZ (Fig. 11a). The distributions, converted to rainfall using Kwajalein’s climatological $Z-R$ relation, show that most of the near-

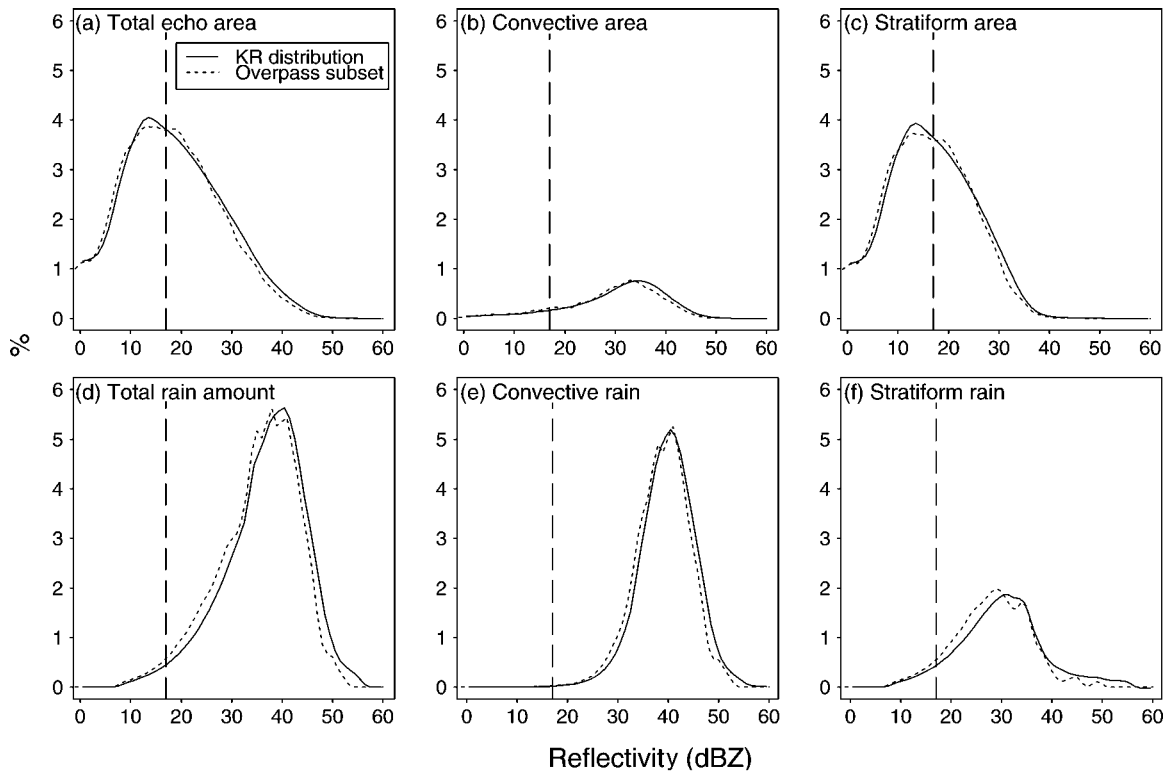


FIG. 11. Frequency distributions comparing KR distributions for Aug 1998–Aug 1999 and the KR overpass subset at near surface. Vertical dashed line indicates the PR 17-dBZ threshold.

surface precipitation occurs when reflectivities are greater than 17 dBZ (Fig. 11d). Reflectivities of less than 8 dBZ are not considered measurable precipitation by the Kwajalein $Z-R$ relation (Fig. 9). Whereas 46% of KR near-surface echo area greater than or equal to 0 dBZ is not seen by the PR because of its sensitivity, only 2.3% of near-surface rainfall is missed. These numbers apply for both the overpass subset and the entire KR period. An additional KR calibration offset of +2 dB (-2 dB) changes these percentages to 40% (53%) and 1.5% (3.4%), respectively; therefore, the percentages are robust to moderate calibration offsets.

The echo area overpass subset (Fig. 11a) undersamples reflectivities greater than 25 dBZ when compared with the entire KR period. The undersampling of higher reflectivities places more emphasis on lower reflectivities, which shifts the rain amount distributions such that the overpass peak of rainfall occurs at a lower reflectivity (Fig. 11d). Figures 11b, c, e, and f illustrate the contribution by the convective and stratiform components to the sampling discrepancies highlighted by Figs. 11a,b. The undersampling of higher reflectivities and thus the shift in distribution by the overpass subset are distributed equally between the convective and stratiform distributions. Otherwise, the convective and stratiform overpass distributions match the total KR distributions nicely.

The KR convective and stratiform reflectivity and precipitation distributions show that stratiform reflectivity dominates the area distribution, contributing 86% to the total area of reflectivity (Fig. 11c), but the convective rainfall dominates the rainfall distribution, accounting for 66% of the total precipitation (Fig. 11e). Convective percentages of rainfall in the Global Atmospheric Research Program Atlantic Tropical Experiment were $\sim 60\%$ (Cheng and Houze 1979); in the Tropical Ocean and Global Atmospheric Coupled Ocean-Atmosphere Response Experiment (TOGA COARE) they were 15%–50% (Yuter and Houze 1998). The much lower fractional convective rain amount in TOGA COARE probably reflects the more frequent occurrence of larger mesoscale convective systems with large stratiform regions in the deep Tropics, over the Pacific warm pool. Kwajalein lies on the fringes of the intertropical convergence zone, in an environment evidently less supportive of mesoscale organization of convection. The relatively higher percentage of convective rain at Kwajalein coincides with the analysis of the rain gauge events (section 4, Fig. 2); that is, long-lasting systems that create large stratiform areas occur infrequently.

9. Diurnal variation in rainfall

Albright et al. (1985) found a weak semidiurnal cycle in this part of the Tropics in infrared satellite imagery. Bedrick and Burgett (1999) found a strong morning peak and weaker evening peak in two years of cloud-

to-ground lightning strike data from four low-gain lightning direction finders located around Kwajalein Atoll. Studies of the TOGA COARE region to the west indicate a stronger diurnal cycle than semidiurnal (Chen and Houze 1997; Sui et al. 1997).

Daily cumulative rain amounts in 3-h periods were calculated for each gauge in the Aeromet and RMI networks for the period August 1998–August 1999 to identify any diurnal variability within the Kwajalein region. Data from three gauges, ranging in latitude from 9.4° to 7.8°N , are shown in Figs. 12a–c (Note: none of the gauges had a complete record during the 1-yr period of accumulation). The bar plots indicate a weak early-morning peak and an even weaker early-afternoon peak for accumulations at each gauge. Lines representing the beginning time of the more intense precipitation events (>10 -mm accumulation) show a double peak at Roi and Loen; there is no signal at Kwajalein (although longer periods of data do show the double peak at Kwajalein). This signal is much less obvious when two months of 10-min samples of KR data are combined.

PR diurnal sampling by the 50 overpasses between August 1998 and August 1999 shows no resemblance to the weak semidiurnal signal seen in the gauge data (Fig. 12d). The bias from undersampled diurnal variability, especially of small-scale phenomena, is most serious in polar-orbiting measurements from a single platform (Salby and Callaghan 1997). The precessing orbit of the TRMM satellite allows for diurnal sampling, but the isolated nature of convection at Kwajalein along with the weakness of the semidiurnal signal does not allow the PR to observe diurnal variability at Kwajalein over the course of the year.

10. Latitudinal gradient of rainfall

The KR rain maps for September 1998 and 1999 were accumulated from 6- to 10-min volumes of KR data (Fig. 13). Overpass subsets of the KR rain maps illustrate the spatial rainfall patterns sampled by the PR. The overpass rain rates were assumed to last 1 h and then were added together; their scales are not meant to represent true monthly accumulations. The lack of PR coverage during a monthlong period is striking. As seen in Fig. 3, it is obvious that just a handful of events determine the monthly PR coverage.

The September 1998 KR rain map indicates a strong latitudinal precipitation gradient spanning the 300-km diameter region covered by the Kwajalein validation site. Accumulations range from 250–300 mm in the southwest to 50–150 mm in the northeast. There was a concern that second-trip echoes (see section 2) could artificially produce such a strong gradient, but gauge accumulations for this month independently corroborate the radar-observed spatial gradient. The sampling by the PR was insufficient to detect the north–south gradient. The September 1999 KR rain map portrays a more homogeneous field, with only the far northeast corner hav-

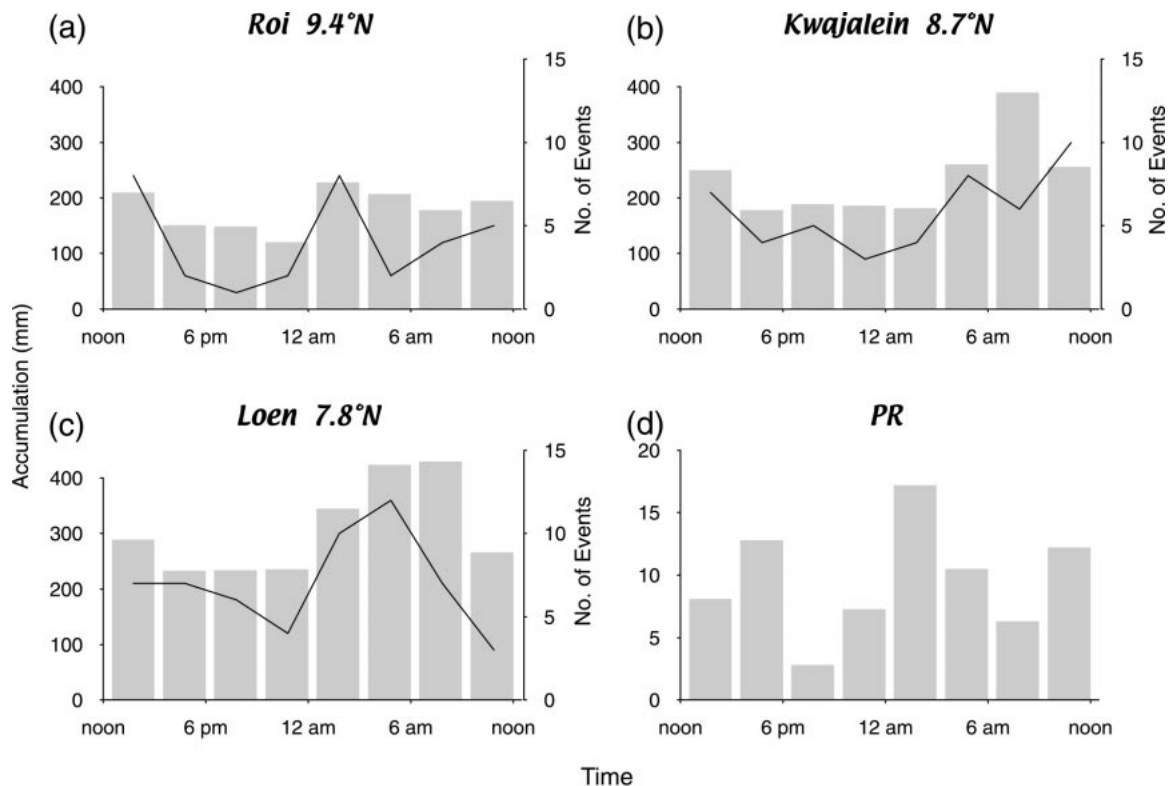


FIG. 12. Rain gauge 3-h accumulations for Aug 1998–Aug 1999 at three gauges within the Kwajalein validation area. The bars indicate rainfall accumulation. The lines show the begin times of events that accumulated greater than 10 mm: The PR accumulations are from the 50 overpass cases binned into 3-h increments.

ing lower accumulations than the rest of the KR area. Gauge accumulations mirror the lack of latitudinal gradient. The PR subset seems to match the spatial pattern of the KR rain map better simply because no obvious pattern exists.

11. Conclusions

The Kwajalein oceanic validation radar and the attenuation-corrected TRMM precipitation radar reflectivity data agree well *within the range of sensitivity of the PR*, that is, for reflectivity values that exceed the PR threshold of 17 dBZ. The convective/stratiform and rainfall-rate fields that are based on reflectivity also compare well within the range of the sensitivity of the PR. Differences between the PR and KR convective–stratiform separation algorithms and Z – R relations do not strongly affect these results. The main distinction between the KR and PR and their ability to capture the instantaneous precipitation field lies in the sensitivity of the PR, which effectively limits it to detecting rain rates ≥ 0.2 – 0.4 mm h^{-1} (15–20 dBZ). Because of the limited sensitivity of the PR, stratiform rain regions and echo associated with ice hydrometeors aloft (anvils) are highly undersampled. The PR misses almost 50% of near-surface stratiform rain area but less than 3% of near-surface stratiform rainfall. Aloft, the PR cannot sense

85% of the ice region. A potentially useful method for detecting the stratiform rain and ice not seen by the PR is to use the KR in combination with the TRMM microwave imager, which sees weaker precipitation and scattering from ice aloft, but with less horizontal and vertical resolution.

A weak semidiurnal signal is evident in 3-h gauge accumulations over a year period. The PR might capture this weak signal after more years of daily sampling. At times, a strong monthly latitudinal precipitation gradient occurred over the 300-km-diameter region centered on the KR. The presence of such a strong north–south precipitation gradient over an area as small as 300 km in dimension over the open ocean is an interesting point from which to study ocean–convection interactions. The PR did not capture this latitudinal precipitation gradient in a month-long period. Longer time periods of study and combining the PR with the TMI rain estimates might make possible the detection of this feature.

With an understanding, based on the KR data, of what the TRMM PR can and cannot see, the use of the TRMM satellite to study the structure of convection and the climatic characteristics of precipitation across the Tropics becomes more realistic. The KR also provides a bound on the errors in sampling by the satellite. The physical understanding and error assessment by the KR

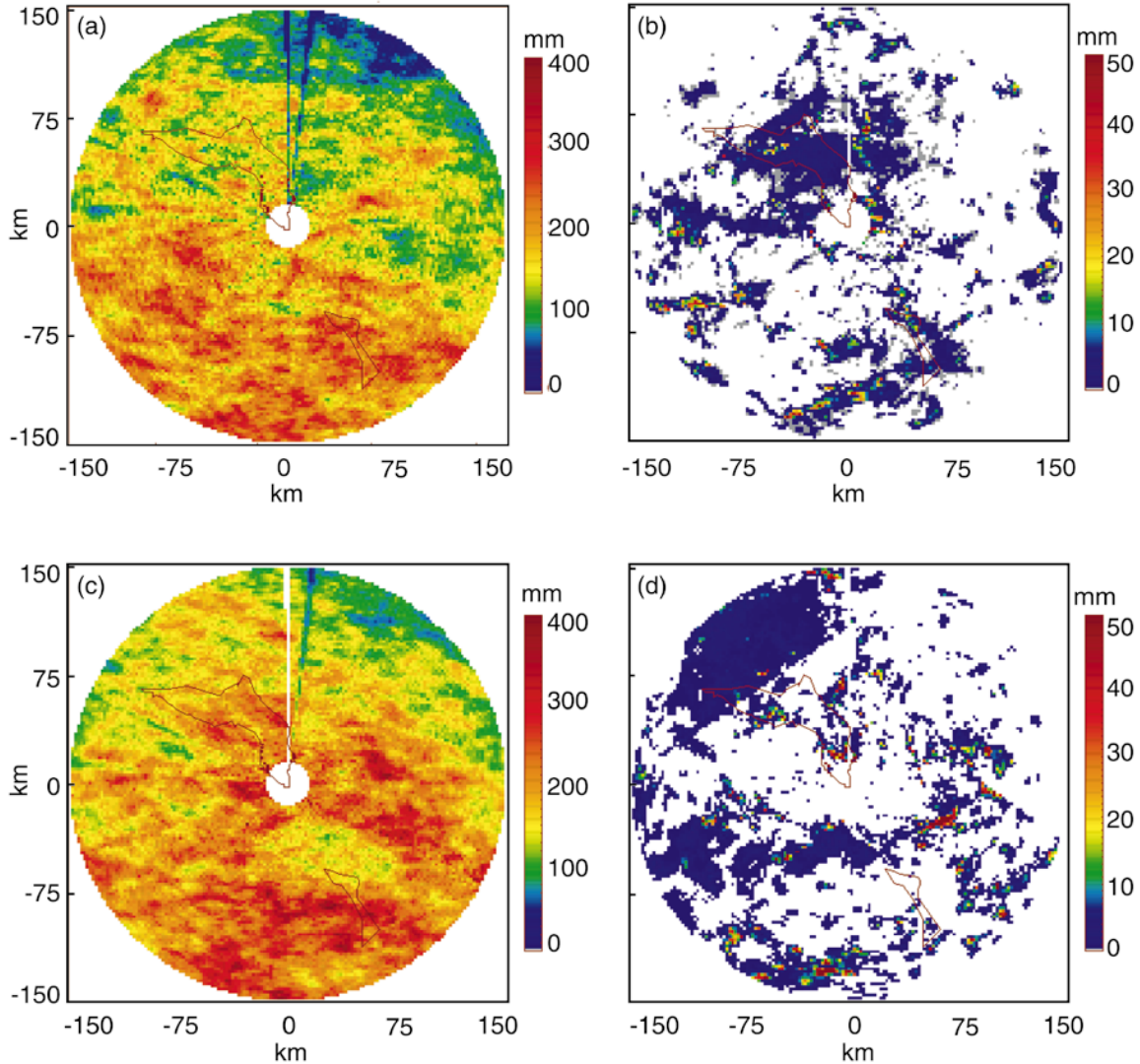


FIG. 13. (a) Sep 1998 KR monthly rainfall map. (b) Cumulative KR rainfall for Sep 1998 overpasses. Instantaneous KR rain rates (mm h^{-1}) were added together for the month, assuming an hour duration for each rain rate. These values are not meant to indicate true monthly rainfall amounts. (c) and (d) As above, but for Sep 1999.

will create a more robust data set for analysis both over Kwajalein specifically and over the Tropics in general.

Acknowledgments. R. Kakar and O. Thiele were responsible for establishing the Kwajalein TRMM oceanic validation site. We thank our TRMM colleagues S. Yuter and C. Leary for their scientific comments, and S. Brodzik, C. Gudmundson, and L. Pratt for their technical support. This research was supported by NASA Grant NAG5-4795.

REFERENCES

- Albright, M. D., E. E. Recker, and R. J. Reed, 1985: The diurnal variation of deep convection and inferred precipitation in the central tropical Pacific during January–February 1979. *Mon. Wea. Rev.*, **113**, 1663–1680.
- Awaka, J., T. Iguchi, H. Kumagai, and K. Okamoto, 1997: Rain type classification algorithm for TRMM precipitation radar. *Proc. Int. Geoscience and Remote Sensing Symp.*, Suntec City, Singapore, Institute of Electrical and Electronics Engineers, 1633–1635.
- Bedrick, M. A., and W. S. Burgett, 1999: A tropical oceanic cloud-to-ground lightning study. Preprints, *23d Conf. on Hurricanes and Tropical Meteorology*, Vol. 1, Dallas, TX, Amer. Meteor. Soc., 243–245.
- Chen, S. S., and R. A. Houze Jr., 1997: Diurnal variation and life-cycle of deep convective systems over the tropical Pacific warm pool. *Quart. J. Roy. Meteor. Soc.*, **123**, 357–388.
- Cheng, C., and R. A. Houze Jr., 1979: The distribution of convective and mesoscale precipitation in GATE radar echo patterns. *Mon. Wea. Rev.*, **107**, 1370–1381.
- Hitschfeld, W., and J. Bordan, 1954: Errors inherent in the radar measurements of rainfall at attenuating wavelengths. *J. Meteor.*, **11**, 58–67.
- Houze, R. A., Jr., 1982: Cloud clusters and large-scale vertical motions in the Tropics. *J. Meteor. Soc. Japan*, **60**, 396–410.
- , 1989: Observed structure of mesoscale convective systems and

- implications for large-scale heating. *Quart. J. Roy. Meteor. Soc.*, **115**, 425–461.
- Iguchi, T., and R. Meneghini, 1994: Intercomparison of single-frequency methods for retrieving a vertical rain profile from airborne or spaceborne radar data. *J. Atmos. Oceanic Technol.*, **11**, 1507–1516.
- Joss, J., and A. Waldvogel, 1990: Precipitation measurement and hydrology. *Radar in Meteorology*, D. Atlas, Ed., Amer. Meteor. Soc., 577–606.
- Mueller, E. A., and A. L. Sims, 1967: Raindrop distributions at Majuro Atoll, Marshall Islands. Illinois State Water Survey Tech. Rep. ECOM-02071-RR1, 1–10. [Available from ISWS, 2204 Griffith Drive, Champaign, IL 61820.]
- Salby, M. L., and P. Callaghan, 1997: Sampling error in climate properties derived from satellite measurements: Consequences of undersampled diurnal variability. *J. Climate*, **10**, 18–36.
- Simpson, J., R. F. Adler, and G. R. North, 1988: Proposed Tropical Rainfall Measuring Mission (TRMM) satellite. *Bull. Amer. Meteor. Soc.*, **69**, 278–295.
- Steiner, M., and R. A. Houze Jr., 1998: Sensitivity of monthly three-dimensional radar-echo characteristics to sampling frequency. *J. Meteor. Soc. Japan*, **76**, 73–95.
- , ———, and S. E. Yuter, 1995: Climatological characterization of three-dimensional storm structure from operational radar and rain gauge data. *J. Appl. Meteor.*, **34**, 1978–2007.
- Sui, C. H., K. M. Lau, Y. N. Takayabu, and D. A. Short, 1997: Diurnal variations in tropical oceanic cumulus convection during TOGA COARE. *J. Atmos. Sci.*, **54**, 639–655.
- Yuter, S. E., and R. A. Houze Jr., 1998: The natural variability of precipitating clouds over the western Pacific warm pool. *Quart. J. Roy. Meteor. Soc.*, **124**, 53–99.